npj | climate and atmospheric science

www.nature.com/npjclimatsci

ARTICLE OPEN

Check for updates

Arctic Oscillation and Pacific-North American pattern dominated-modulation of fire danger and wildfire occurrence

Flavio Justino[1]✉, David H. Bromwich[2], Vanucia Schumacher[3], Alex daSilva[4] and Sheng-Hung Wang[2]

Based on statistical analyses and Arctic Oscillation (AO) and the Pacific-North American pattern (PNA) induced climate anomalies in the 2001–2020 interval, it has been found that these climate modes drastically influence the fire danger (PFIv2) in differing ways across coastal and inland regions. The AO induces higher fire risk in northern Eurasia and central North America, whereas the PNA increases the fire danger across southern Asia and western North America. Moreover, fires have been predominantly identified, up to 70%, during the positive phases of AO and PNA northward of 50°N, in particular over Alaska, Baltic States and eastern Asia. For coincident positive AO and negative PNA days, a large number of fires have been identified over northwestern North America and northern Eurasia. Spectral analyses demonstrate that weather anomalies related to AO and PNA lead fire danger by 10–20 days, and both modes are significantly correlated to PFIv2 over north America and most of Eurasia. Despite some drawbacks related to the fire danger methods currently applied (PFI and FWI), it is demonstrated that the influence of AO and PNA on potential environmental driven-fires can be anticipated, in some locations on almost 90% of days. Fire danger forecasts are urgently needed and the understanding of factors and conditions, which are able to modify the environmental susceptibility to fire development, are crucial for adequate management to reduce the harmful effects of fire. In this sense, our results reveal that a better prediction of the fire season can be achieved by advanced assessment of the PNA and AO behavior, and shed light on the need to investigate the impact of other modes of climate variability upon wildfire frequency and severity.

npj Climate and Atmospheric Science (2022)5:52 ; https://doi.org/10.1038/s41612-022-00274-2

INTRODUCTION

At the forefront of global issues, the frequency and severity of wildfires emerge as threatening events, not only for the livelihood of people but also for infrastructure and environmental sustainability[1–5]. Seasonality is the primary cause for local distribution and severity of wildfires, but large fluctuations in the spatial and temporal distribution of fire occurrence have been observed[6–8]. Summer climatic conditions across the Pan-Arctic region and extra-tropics, exhibit features which are conducive to fire activity due to dry and warm conditions[9]. This is not a particular characteristic of Boreal latitudes, as the tropics in summer are also prone to wildfire occurrences[2,10] due to warm and dry conditions. In both regions, precipitation distribution is not uniform throughout spring-summer, and high temperature and low precipitation lead to reduced soil moisture affecting local vegetation properties such as productivity and greenness[11–13].

In addition, surface characteristics are modified by intra-seasonal and daily weather variability[14,15], further contributing to the amount of combustible material, and the environmental fire danger[16,17]. It is worth mentioning that based on the fire weather index (FWI), significant upward trends in fire danger[6] have been found over more than a quarter of global burnable land masses for the 1979–2020 interval. Anthropogenic climate change has also been responsible for 55% of observed increases in fuel aridity from 1979 to 2015 on wildfires across western United States (WUS) forests[18]. In 2020 during the fire season across the WUS, 50% of increased vapor pressure deficit has been attributed to anthropogenic warming[19].

Examination of the relationship among drivers of vegetation fires as well as their response to large-scale climate modes (departure from mean conditions), provides insights into the processes responsible for fluctuations of the fire regime in the time–space domain[20]. For instance, the El Niño-Southern Oscillation phenomenon has been related to global fire incidence due to meteorological anomalies associated with teleconnection patterns[21,22]. The Southern Oscillation Index from June to November in the year before a fire event may be applied in association with past precipitation, to predict wildfire area in Australia[23]. Variability of subtropical and extratropical climate modes have been linked to pronounced fire seasons as well. Dixon and collaborators[24] found statistically significant correlations between the number of fires and the Pacific-North American pattern (PNA) in southern United States. They argue that July PNA-induced weather anomalies are crucial to the upcoming fire season of late summer and autumn. The increased severity of Siberian fires over the past decades has been attributed to a reduction of summer precipitation, triggered by a recurrent positive phase of the Arctic Oscillation in May[25]. Moreover, interannual forest fire variability in Central Siberia is highly associated with a combination of the Arctic Oscillation (AO) index and regional summer temperatures. The association between fires and climate indices may exhibit a lead–lag relationship. It has been found that the annual burned area increases when a positive AO dominates in early months of the year, though peak fire season takes place 1–2 months later[26].

Despite great effort to understand climate mechanisms related to fire characteristics, most studies deal with realizations that are primarily focused on a particular region or time. This has been partially alleviated by recent studies addressing those issues over the global domain[6,27]. In particular, Shi and Touge[27] used several climatic indices to characterize drivers of spatio-temporal patterns

[1]Departamento de Engenharia Agrıcola, Universidade Federal de Vicosa, Vicosa, MG, Brazil. [2]Byrd Polar and Climate Research Center, The Ohio State University, Columbus, OH, USA. [3]Instituto Nacional de Pesquisas Espaciais, Sao Jose dos Campos, Sao Paulo, Brazil. [4]Universidade Federal do Oeste do Para, Instituto de Engenharia e Geociencias, Santarem, PA, Brazil. ✉email: fjustino@ufv.br

of burned areas. Among other results, they demonstrated a significant contribution of PNA weather anomalies to increased burned area over central Eurasia.

The PNA and AO, which vary continuously in time, stand out as appropriate candidates as fire drivers because they are associated with large anomalies in surface temperatures, precipitation, and extreme events across North America and Eurasia. Indeed, the AO induces in most of the Northern Hemisphere positive temperature anomalies, which are enhanced by the PNA contribution across Eurasia[15,28–30]. These modes are mostly treated as individual manifestations of climate. However, they can also act simultaneously to modify local environmental conditions by coupling atmospheric, oceanic, and land surface processes[31]. Therefore, in the current study great effort is dedicated to determine the impact of PNA and AO in influencing fire characteristics during the 2001–2020 interval. Moreover, the ratio of satellite-detected fires in distinct phases of those indices are determined. Future climate is expected to be modified by changes in the AO and PNA, substantially affecting atmospheric conditions across the extratropics[32]. Thus, global warming perspectives increase the necessity to investigate the critical sensitivity of the Arctic environment to climate change. Local fires, which intensify the atmospheric greenhouse gas feedback, have to be in the priority chain for transdisciplinary studies[1,7,33].

RESULTS

Pattern of fire-weather components: precipitation and temperature

Analyses in the following are primarily based on climate composites and statistical analyses. The relationship between the climate impacts induced by the AO and PNA on hotspots are also explored. Initially, fire weather characteristics are investigated to identify preferential fire danger patterns, in terms of temperature and precipitation. This analysis aims to identify regions which are differently affected by daily fire weather features, despite having homogeneous climate conditions on monthly and annual timescales. According to Table 1 only in 10% of analyzed cases does a region experiences days in which both indices show simultaneous positive values.

Figure 1a–d shows composite characteristics associated with the positive phases of AO and PNA. These anomalies (deviations from 20 years daily climatology) are constructed based on 15-day running average precipitation and temperature for positive AO and PNA, for indices larger than 0.5 standard deviation. The ASRv2 is used for the 2001–2016, and ERA5/CPC for the 2001–2020 intervals. During positive AO, the central part of North America (NA) exhibits drier conditions, whereas most of the east and west coast and northern Canada show modest precipitation changes by up to 0.5 mm/day (Fig. 1a). Influence of the AO is stronger in Eurasia, where the western part and the far east of the continent experience a drop in precipitation; higher rainfall is noticed in northern Russia and Scandinavia, in particular.

Turning to PNA (Fig. 1b), it is clear that with respect to anomalies induced by the AO, precipitation changes in NA are more affected. Drier conditions are present in western Canada/US and across northern Canada, which parallel the impact of the AO, leading to dryer vegetation, thus more conducive to fire. Over Eurasia (Fig. 1b), changes are weaker but in general northward of 50°N positive precipitation anomalies are found. On one hand, this favors large water availability and lower fire danger, but on the other hand, this also increases the amount of vegetation cover which acts as combustible material for fire development. This is the case associated with extensive fires in Siberia[26]. It is found that positive AO in early months of the year is highly correlated to increased extension of annual burned area.

The impact of PNA on temperature shows over Alaska and the central/eastern part of NA, a seesaw pattern (Fig. 1d), in which temperature increases in the former, but decreases in the latter region. Similar out-of-phase characteristics between Alaska and Canada is found by investigating the frequency of hottest days (Txx) across North America[9] related to the AO patterns. The AO induces across Eurasia the presence of a warm core over northern Russia which gradually weakens outwards, but no notable cooling is indicated (Fig. 1c). These features are induced by internal atmosphere–land interactions sensitive to both snow cover and soil moisture anomalies in the spring[11,34]. This region in Siberia experiences a large number of fires, and between 90°E–120°E, positive trends in hotspots have been observed in the last two decades[35].

Across central and eastern Asia during the positive phase of the PNA, remarkable warming with values up to 2 °C are observed (Fig. 1d). This increase in summer temperatures related to the PNA, may arise from interactions with other dominant climate modes of variability in the northern Pacific, such as the Western Pacific pattern[36]. The most important component inducing higher danger rating in the extratropics is the period of drought (DD, see methods, Fig. 1e, f). This feature takes into account the distribution of precipitation in distinct intervals during the preceding 120 days[35]. The DD is correlated with running averaged-15-day precipitation, but considers the long memory of rainfall episodes within 4 months.

Increases in DD indicating dry conditions during the PNA$^+$ phase are noticed over central and western NA (Fig. 1f). In Eurasia the pattern is dominated by two areas of strong out-of-phase variability over central Eurasia/Europe and northern Russia (Fig. 1f). Indeed, mid-latitudes in Eurasia experiences a large increase in DD (reduced short-term precipitation), whereas the northern portion of the continent (Siberia) is characterized by decreased DD (increased 120-day precipitation amount).

By comparing the hemispheric picture, the DD composite associated with the AO$^+$ and PNA$^+$ (Fig. 1e, f), reveals that the PNA$^+$ plays the leading role in modifying the 120-day precipitation distribution in NA, inducing dry conditions in the north and western parts. Across Eurasia, the DD spatial patterns exhibit many similarities, but magnitudes related to the AO$^+$ are larger with respect to changes related to the PNA$^+$. This points out the importance of the PNA and AO not solely to weather, as previously found[37,38], but to fire potential as well.

Table 1. Percentage of days with positive or/and negative phases of PNA and AO for indices larger than 0.5 standard deviation from March to October during the 2001–2020 interval.

Index	AO+	PNA+	AO−	PNA−
PNA+	10	27	7	–
PNA−	6	–	9	28
AO+	29	10	–	6
AO−	–	7	28	9

PFIv2 and FWI characteristics related to the AO/PNA

After discussing fire-weather conditions, the response of PFIv2 and FWI to the AO/PNA is now analyzed. This is important because the inter-annual variability of the fires can be related to a preferential phase of these modes. Daily weather changes due to the AO and PNA have long been recognized and extreme summer temperatures can be induced by the AO and PNA[30,39,40]. These modes of climate variability interact with surface characteristics by modifying soil moisture and subsequently vegetation dynamics[41]. This last study particularly pointed out that most recent increase in the frequency of wildfires in central Siberia matches a reduction of

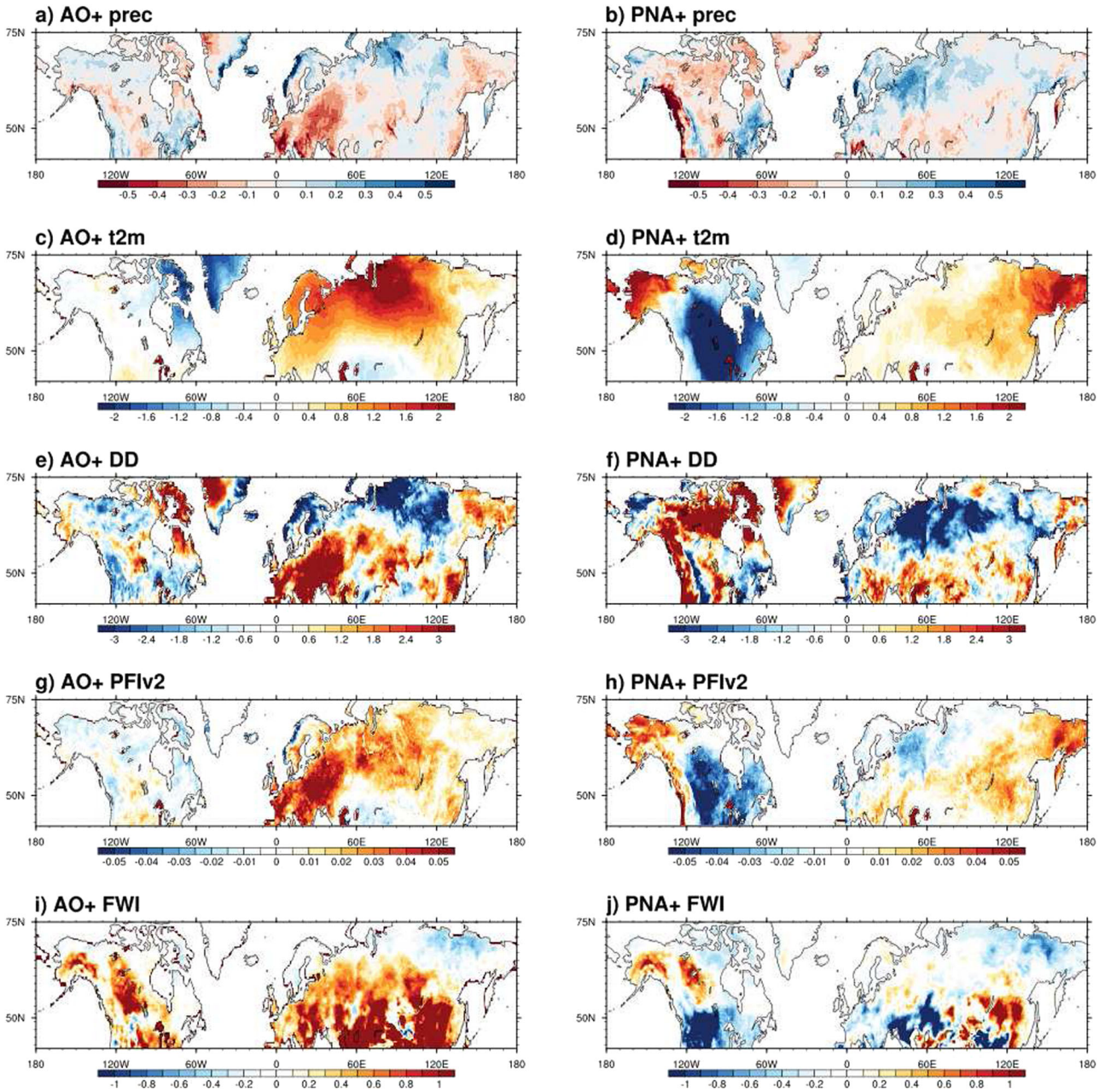

Fig. 1 Composite patterns due to AO+ and PNA+. a, **b** precipitatiom (mm/day), **c**, **d** surface temperature (*C*), **e**, **f** period of drought, **g**, **h** is for the PFIv2, **i**, **j** for the FWI. AO+ and PNA+ exceed 0.5 standard deviation.

summer precipitation, triggered by a positive phase of the AO in May.

Figure 1g–j shows changes of PFIv2 and FWI associated with positive AO and PNA. These two fire danger rating indices have been used to estimate the environmental vulnerability to wildfires, over the tropics and extratropical regions[10]. The pattern in PFIv2 is mainly dictated by changes in DD, but an important contribution to fire danger rating is due to temperatures, in particular over northern Eurasia, east Asia and NA (Fig. 1c, d, g, h). Elsewhere, short-term changes of precipitation as represented by DD dominate the PFIv2. Two regions under higher magnitude anomalies are identified in western North America and Europe/central Russia, which indicate marked regional fire vulnerability related to AO and PNA. As previously mentioned, the AO^+ dominates the PFIv2 anomalies in Eurasia whereas the PNA^+ shows stronger influence across NA. It may be argued that the fire-weather features in Alaska and Siberia do not concomitantly occur in response to AO^+ and PNA^+ (Fig. 1g, h), since those indices are barely correlated.

The FWI composite anomalies (Fig. 1i, j) shows differences in the regional distribution with respect to PFIv2. For instance, the FWI delivers large positive anomalies across North America, which is a response to increased water vapor deficit and the seasonal lack of precipitation, mostly related to AO, over the Canadian sub-Arctic woodland tundra, northern woodland and northwest forests (Fig. 1i). These are regions that experience a significant number of fires (see Fig. 5a).

Turning to Eurasia, the FWI and PFIv2 show many similarities with respect to their response to the AO but the FWI and PFIv2 diverge across southern and northern Asia for PNA^+. The FWI is affected by precipitation whereas the PFIv2 strongly responds to temperatures. Strictly speaking, regional differences in the pattern

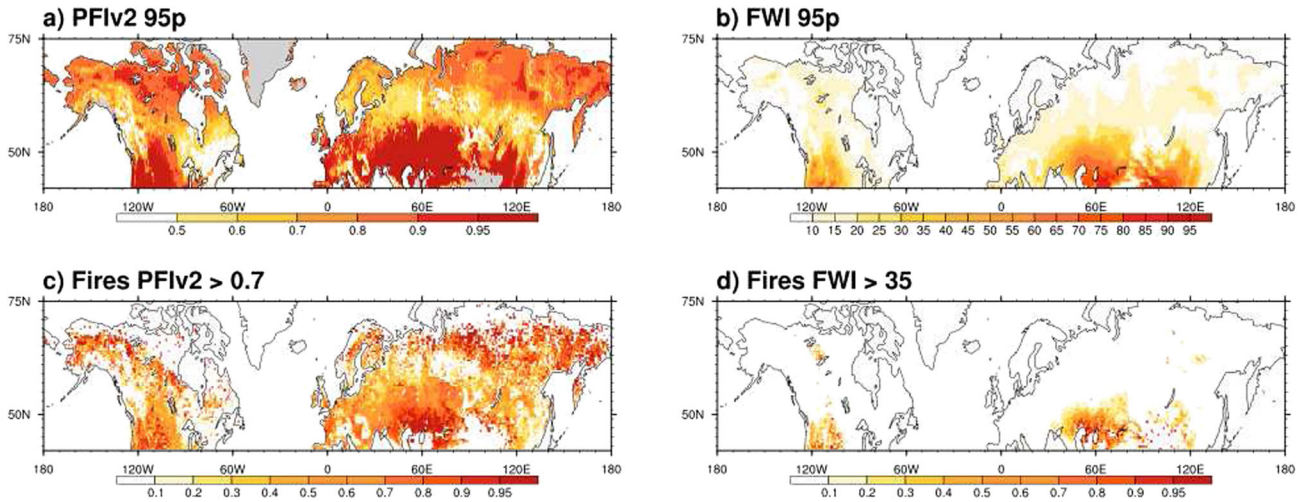

Fig. 2 Extreme fire danger and observed fires. 95th percentile based on daily values of PFIv2 (**a**) and (**b**) for the FWI based on 2001–2016 interval. **a**, **b** Are shown in different scales. **c** and **d** show the ratio of satellite-detected fires with respect to the total accumulated in 2001–2016 for PFIv2 > 0.7 and FWI > 35 (high danger ratings).

of variability may also result from the use of high frequency precipitation, because the FWI uses accumulated 24 h precipitation values in the calculation, which vary considerably, whereas the PFIv2 applies a precipitation factor that varies at much lower frequency (120 days). This is shown in Fig. 2 by regions where both fire danger indices deliver values above the 95th percentile. This is important since fires are expected to be found over areas with PFIv2 larger than 0.7, and FWI values above 35. It is clear that higher values of PFIv2 are found at most locations in the extratropics, but they are confined to 40–50°N in FWI. It is suggested that in FWI the scaling levels (see the "Methods" section), to indicate high fire danger ratings should be modified to represent extratropical patterns. The current scale is not able to locate fires and proper FWI ratings together. This is shown in Fig. 2c, d. In PFIv2, more than 60% of MODIS-based fires in the 2001–2016 fall within danger rating higher than 0.7 whereas in FWI >35 fires are concentrated only across the subtropics.

Temporal variability of PFIv2 and FWI

Several studies have been conducted to characterize the temporal relationship between surface conditions and the extra-tropical modes of climate variability. In additional effort, this issue is currently addressed (Fig. 3) based on the maximum correlation between the AO, PNA and the fire danger indices as well as the associated lag of occurrence. The power spectrum and the co-spectrum variance and coherence squared are also explored.

Maximum correlation may be as high as |0.5| over Europe and Asia. In general, most significant correlations are associated with the AO and PNA over Eurasia (Fig. 3a, c). For the AO, positive values are noticed over western NA, and negative correlation are found across the eastern part, corroborating the precipitation pattern shown in Fig. 1a. Across most of Eurasia the AO^+ is positively correlated with the PFIv2, with significant values as high as 0.5. Magnitude of correlations related to the PNA^+ is more representative over eastern Asia and western NA primarily due to induced warmer conditions (Fig. 1d).

The AO leads PFIv2 anomalies in lags not larger than 10 days (15-day running mean) in NA, and around 25 in Europe and some parts of Eurasia (Fig. 3b). Analyses for PNA indicate longer delay across NA (up to 30 days, Fig. 3d), and eastern Asia (up to 20 days, Fig. 3d). Climate composites indicate that temperature is mainly responsible for the hemispheric correlation pattern due to changes in AO^+ and PNA^+, whereas precipitation plays a significant role for the regional distribution.

Turning to FWI, it is clear that Fig. 3a, c, e–g display different characteristics in particular across Eurasia. Over most of Asia, PFIv2 and FWI have inverse PNA and FWI correlations, which is corroborated with composite anomalies shown in Fig. 1g–j. Moreover, the time response of those indices to PNA and AO is different. In fact, the FWI requires a longer time to achieve the maximum response (highest correlation), about 20 days for both modes. It should be argued that this feature is related to the formulation of the indices, especially in terms of precipitation. In PFIv2, precipitation evolves over 120 days taking into account gradual dryness of soil and vegetation, whereas the FWI is a function of drought and fuel moisture codes, that require a longer response time. This interaction among parameters can be responsible for the FWI delayed response to AO and PNA. Thus, the predictability of fire danger as derived from weather patterns is demonstrated to be a function of the fire danger model used.

The temporal relationship between the PNA, AO, PFIv2, and FWI is further evaluated based the power spectrum and the co-spectrum variance and coherence squared (Fig. 4 and Supplementary Fig. 1). The co-spectrum variance measures the extent to which exist oscillations with the same phase between AO/PNA and PFIv2, (or with opposite sign with a phase shift of half a cycle). It indicates the contribution of different frequencies to the total cross-covariance at zero lag. The coherence represents correlation coefficient except that the coherence squared is a function of frequency. It is important to mention that PFIv2 and FWI exhibit different power spectrum characteristics, in which the FWI is dominated by much longer periodicity (Supplementary Fig. 1d). For the PFIv2 and FWI the power spectrum is computed based on the first EOF principal component (Fig. 4). The EOF domain has been chosen according to maximum amplitude of the first harmonic, as shown in Supplementary Fig. 2 for satellite-observed fires. Across North America, this is performed on 40°N–60°N, 130° W–90°W, and in Eurasia over 40°N–60°N, 30°E–150°E.

The PFIv2-dominant pattern shows maximum variability across central Canada and Eurasia, but lower amplitudes in Alaska and northeastern Canada, Scandinavia and southern Asia (Fig. 4a, b). It explains in North America and across Eurasia 19% and 12% of the variance. These AO, PNA and PFIv2 power spectra (Supplementary Fig. 1) do reveal a dominant temporal variability centered at 10–20 and higher than 60 days. For PNA, the 10-day peak insofar as the 99% level is concerned, is weaker and less significant (Supplementary Fig. 1b). However, AO and PNA show a co-spectrum in phase at approximately 10–15-day periodicity, and with

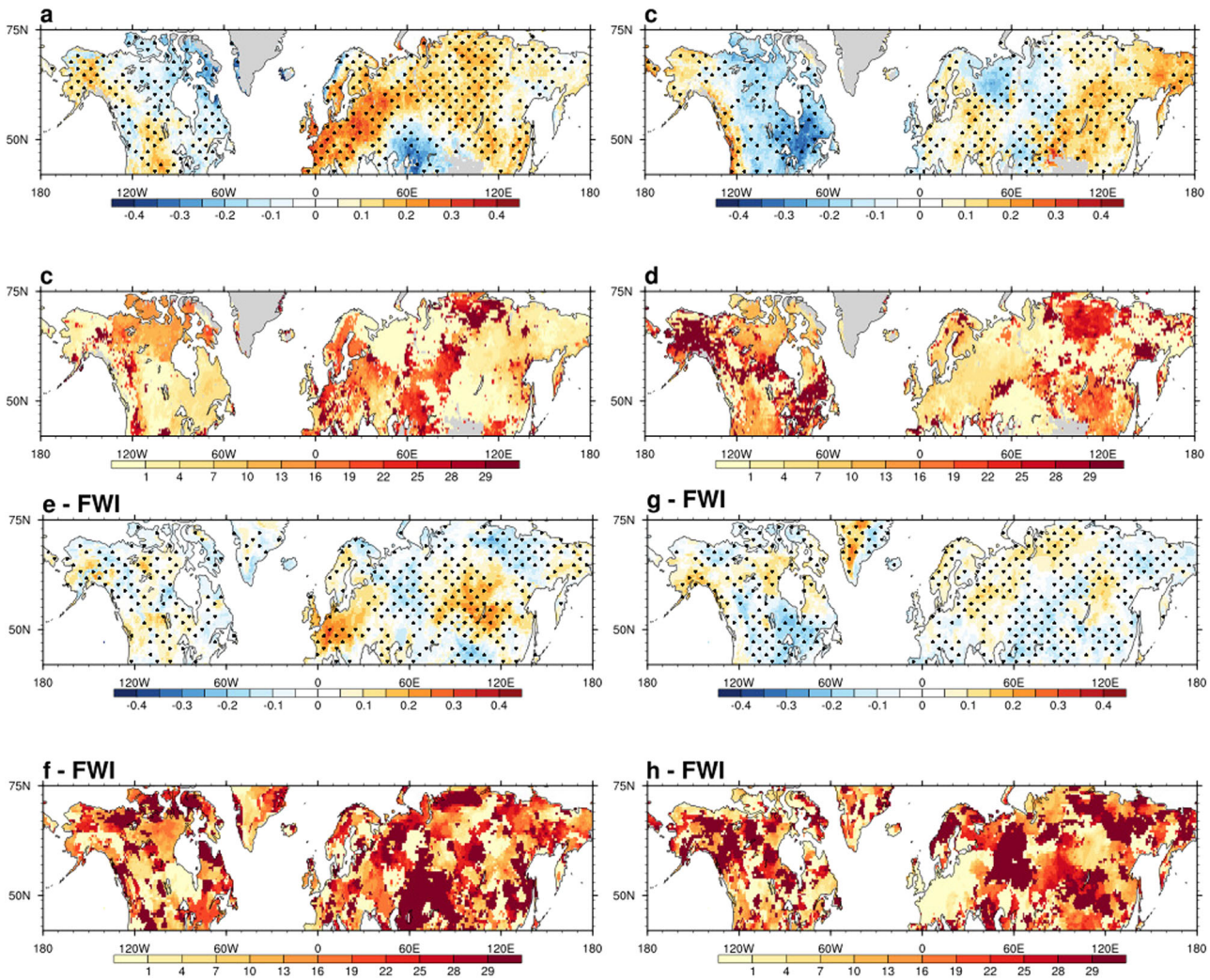

Fig. 3 Correlation analyses between AO/PNA and fire danger ratings. Maximum correlation between the AO and PFIv2 (**a**) and between the PNA and PFIv2 (**c**). **b** and **d** show the lag in days when the maximum correlation occurs. **e**–**h** are the same as (**a**–**d**) but for the FWI calculations. Dotted regions are significant at 95% level. Reddish grids indicate larger lags.

coherence squared by up to 0.4 (Supplementary Fig. 1d, e). To investigate in more detail, a bandpass filter has been applied to filter out frequencies higher than 20 days. This allows to evaluate the relationship between the climate modes and the fire danger in a small temporal window no longer than a month.

The AO and PFIv2 co-spectrum exhibits a dominance of temporal scales by about 10 and 20 days (0.1, 0.04 cycles/day (Fig. 4c, e)), and maximum coherence squared by around 0.05 cycles/day (or ≈20 days Fig. 4g). It should be noted that the correlation map shown in Fig. 3 is based on grid point correlations, whereas co-spectrum characteristics are based on a hemispheric domain. The PNA and PFIv2 shows a co-spectrum similar to that delivered by the AO (Fig. 4c, e) but with lower magnitude (Fig. 4d, f).

The dominant hemispheric pattern of AO and PNA may be assumed to lead the PFIv2 by 15–20-days (Fig. 4a, b). However, estimates as to the local relationship between those features should consider grid point correlations as well (Fig. 3), because grid points will be affected by distinct local anomalies of weather and fire danger rating. Despite PFIv2 and FWI drawbacks, examination of these large-scale spatial patterns of fire danger is important because they can provide information on the local impacts of remote climatic influences, in particular whether seasonal forecasts are practical.

Satellite-based fire characteristics and AO/PNA

After investigating the climatic characteristics of fire related-weather parameters and fire danger, the number and spatial distribution of fires are now discussed. In most cases fires are assumed to be more frequent in summer, however, in some regions weather characteristics in spring and fall may lead to fire occurrences. Fourier analyses conducted to characterize the annual and semi-annual cycles of fires, i.e. how they are distributed throughout the year, reveal that the two harmonics explain most of the variance (Supplementary Fig. 2). In Alaska, the wildfire season is essentially June–July, with shoulders occasionally in May and August. Canada's wildfire season also peaks in the summer. This is noted because the variance of the first harmonic exceeds 40–50%. In Eurasia, the annual cycle is more dominant as compared to the NA as shown by larger variance values (Supplementary Fig. 2), and fires are found from March (over 60° N) to September (elsewhere). Over the 40–50°N belt, fire occurrence seems to be related to agricultural activities and lightning, that do not match the peak of drought and temperatures, as shown by the variance of the second harmonic larger than 50% (Supplementary Fig. 2).

Figure 5 shows accumulated fire at individual grid boxes from 2001 to 2020. Over NA three preferential regions are identified over the Yukon river watershed in Alaska, the Pacific Ocean

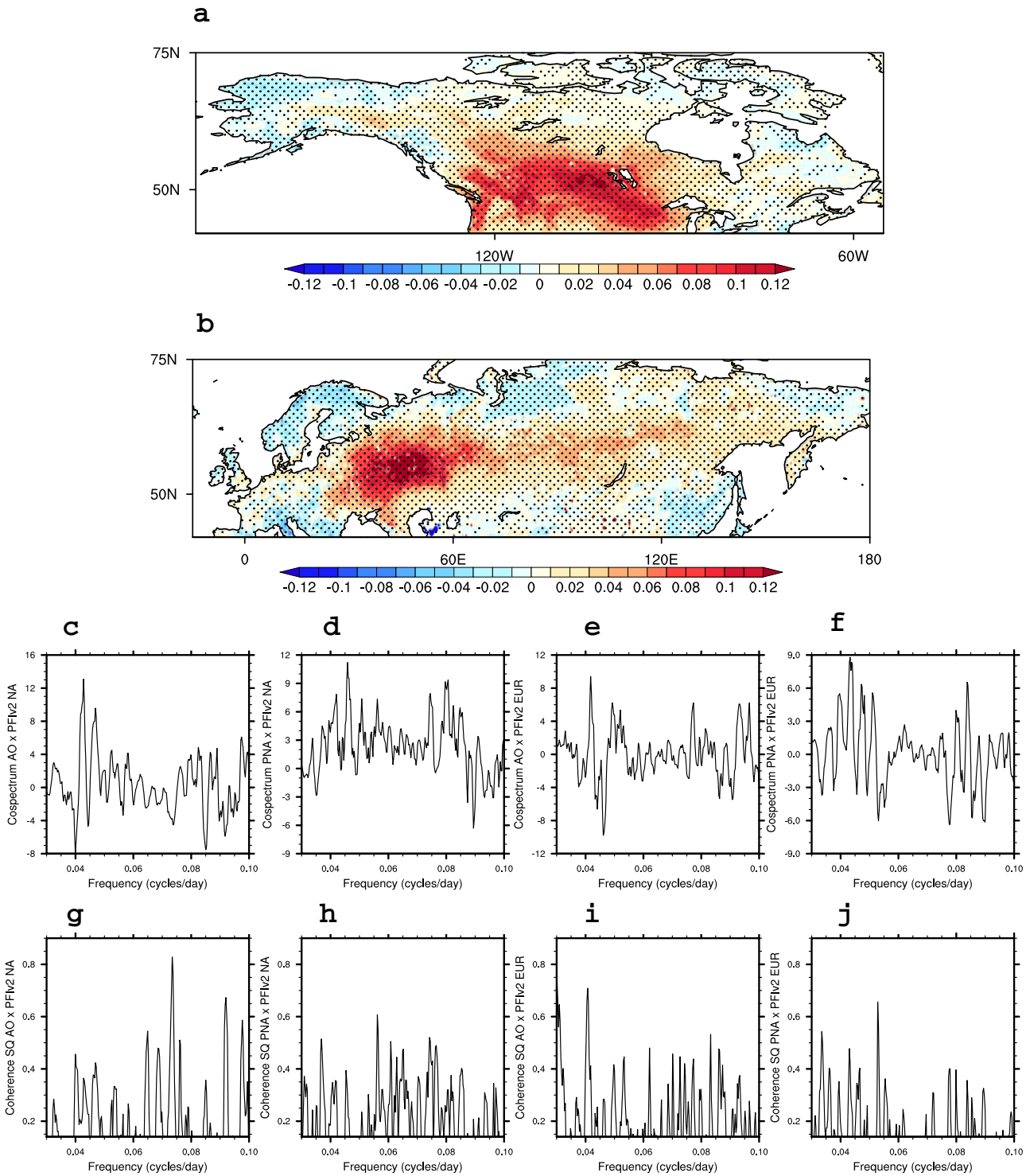

Fig. 4 Dominant PFIv2 pattern and co-spectrum analyses. March–October dominant pattern of PFIv2 as defined by the first EOF (**a**, **b**) computed over the 20°–90°N, 0°-360°. The patterns are displayed as amplitudes by regressing regional NA and Eurasia anomalies upon the standardized first principal component time series. Dotted regions are significant at 95% level. Panels **c** shows co-spectrum between AO and PFIv2 over NA, **d** for PNA and PFIv2 over NA, (e) AO and PFIv2 over Eurasia and **f** PNA and PFIv2 over Eurasia. **g**–**j** are the same as **c**–**f** but for the coherence squared.

seaboard and centered at 58°N-105°W. Over Eurasia, fires are concentrated across the Balkans, the 55°N latitudinal belt and southeastern Asia. The strategy to quantify fires which are most likely influenced by modes of climate variability, is based on the ratio of fires found on days when the AO and PNA exhibit values >0.5 standard deviation to the total accumulated. This reveals that most fires occur in the positive phase of the AO (60%) across Canada (Fig. 5a, c).

By comparing Fig. 5c, d it is noticed that the AO exerts a very important role over Eurasia. This is reasonable because the mode's annular structure induces in those regions, positive (negative) anomalies of surface temperature (precipitation),

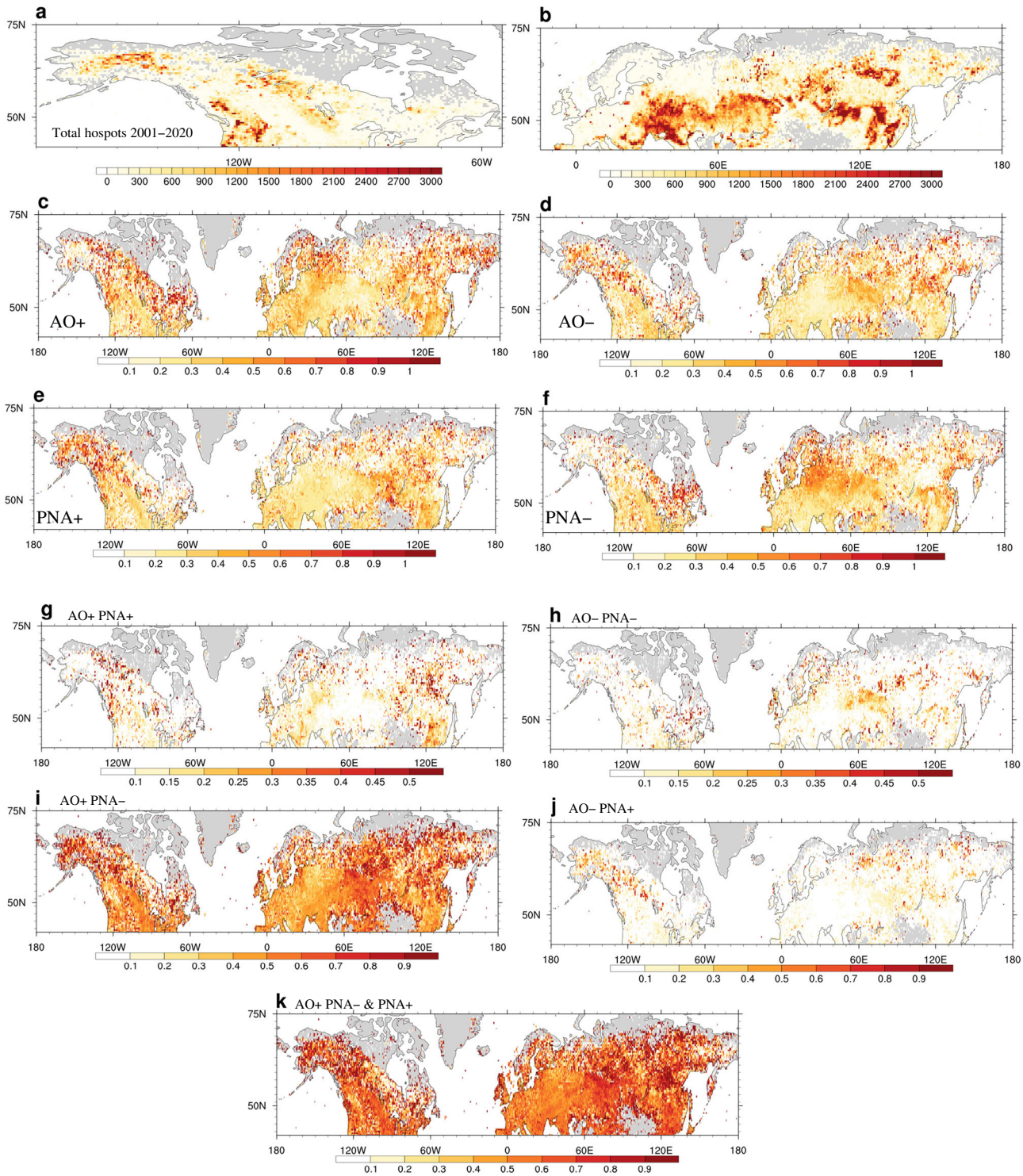

Fig. 5 Fire distribution and AO/PNA. Accumulated number of satellite-observed fires between March and October during 2001–2020 (**a**, **b**). **c** and **d** shows the ratio between fires during AO+, AO and the total accumulated in the period. **e**, **f** is the same as (**c**), (**d**) but for PNA+ and PNA. **g** Shows the ratio but for AO+ and PNA+ and **h** for AO and PNA. **i** AO+ and PNA. **j** AO and PNA, **k** is the sum of (**g**) and (**i**). Labels in **j** range from 0.1 to 0.5.

that in case of persistent anomalies further increase the combustible material and fire danger. The relationship between the AO and fire occurrence during the negative phase, is weaker because Arctic air reaches mid-latitudes. Cold spells in Eurasia and Siberia have been frequently related to negative AO[42]. Advection from the Arctic reduces surface temperature and increases relative humidity making less conducive for ignition and fire propagation (Fig. 5d). In several locations, large concentration of fires occurs under higher fire danger as may be seen in Fig. 2. However, because the PFIv2 does not include all dimensions of fire forcing factors, the effect of AO and PNA on weather conditions can be associated with reduced fire danger with respect to mean conditions in summer.

The PNA is well known for strongly impacting climate conditions over North America, which may modify the frequency of fires, in particular, over Alaska and northwestern Canada. Indeed, more than 60% of fires coincide with PNA^+ (Fig. 5e).

Moreover, positive PFIv2 temperature anomalies occur over these regions as shown in Fig. 1. Lag correlation also illustrates that the PNA leads the fire danger (PFIv2) by 25–30 days (Fig. 3d). Increased precipitation and reduced DD are found during PNA^+ over Alaska and northern Asia, which may favor increases in litter decomposition and fuel accumulation allowing for larger and more severe fires (Fig. 1b, f). For PNA^-, fires are concentrated on the Atlantic seaboard region of Canada, the Baltic states and central Asia (Fig. 5f). Maximum fire danger and fire occurrences are found mostly in phase with lag between 0 and 5 days (Fig. 3d), in particular in the latter region.

To verify in more detail the relationship between the fire frequency, the AO and PNA, Fig. 5g, h shows patterns when both modes are in positive and negative phases with values that exceed 0.5 standard deviation (STD). It stands out that it is rare for a region to experience days in which both indices show negative values at the same time (Fig. 5h); 9% of analyzed days, as shown in Table 1. Positive conditions as well occur in 10% of analyzed days (Fig. 5g) but this is important because about 30% of fires have been detected over northern Canada, southern Asia and eastern-most Russia for coincident AO^+ and PNA^+. The association between the climate modes with fires can also be observed for AO^+ and PNA^- (Fig. 5i). Northern NA and most of Asia experience higher number of fires (up to 70%) when AO^+ and PNA^- are in phase, which occurred in the 2001–2020 interval only during 6% of days. Fires are lesser frequent for simultaneous AO^- and PNA^+ but danger should be monitored in northwest NA and northern Asia (Fig. 5j).

A major finding arising from analyses of the occurrences of fires and positive or negative PNA and AO^+, this demonstrates that AO^+ is crucial to the presence of fires (Fig. 5k). In some locations, such as northern-eastern Asia and northwest North America more than 90% of hotspots are concentrated in days when the AO and PNA indices exceed 0.5 STD. This highlights the importance of monitoring in advance the persistence of the AO^+ and PNA^- acting in conjunction, because weather features under these conditions have been demonstrated to be highly conducive to frequent fires (Fig. 5i).

The climate patterns during the positive phase of those modes (AO^+ and PNA^+, Fig. 6a–e) show increased geopotential height over western North America, northern Europe and central/Eastern Asia imposing dry conditions but lower temperatures in NA (Fig. 6b–d). In Eurasia a different pattern is observed with higher temperatures and increased precipitation, and drop in DD (Fig. 6c, d). Important to mention that in association with warmer temperatures and increased combustible materials related to large amount of trees, shrubs, grasses and cropland leaves, surface conditions related to the AO^+ and PNA^+ interaction are associated with enhanced fire danger in most of North America, northern Eurasia and southernmost Asia (Fig. 6e). However, some regions experience negative/reduced fire danger rating, for instance in western part of NA and large parts of east and south Asia. Over Asia the increase in precipitation is very significant (Fig. 6c, d) under AO^+ and PNA^+ days.

The weather composite based on AO^+ and PNA^- is shown in Fig. 6f–j. These conditions result in a large number of fires despite being present only in 6% of days during the 2001–2020 interval. It is clear over NA that changes in the PNA phase dominate the geopotential response, and also modify the atmospheric circulation in Eurasia (Fig. 6f–i). Main characteristics of these patterns are noticed, furthermore, by lower temperatures, such as over northern and western NA, and parts of southern and eastern Eurasia (Fig. 6g). Opposite temperature response is found over most of NA due to PNA^-, and northern Eurasia primarily resulting from the AO^+ phase. Over these regions temperature increases attain values as high as 3 °C (Fig. 6g).

Changes in daily precipitation and potential impact in the fire activity under AO^+ and PNA^- is reproduced by the DD distribution (Fig. 6h, i). Induced positive anomalies of DD are found over most of Eurasia due to the drop in precipitation (Fig. 6h, i). The DD pattern in NA exhibits more regional features. For instance increased precipitation in the west coast leads to reduced DD, whereas the center and northeastern parts of Canada and Alaska are dominated by positive DD anomalies (Fig. 6h, i). Thus, it is very clear that the joint effect between AO^+ and PNA^-, intensifies the fire danger ratings, in Eurasia as shown by the PFIv2 composites.

Despite the fact that AO^+ and PNA^- may reduce the fire danger ratings, in some cases reduced danger is not sufficient to avoid fires, because precipitation contributes to increase the land cover and dry matter production. These conditions in late spring–early summer, provide the fuel needed for fire development throughout the fire season. It is crucial to stress that the environmental susceptibility to fire is a condition that has to be analyzed in association with additional local conditions, involving people behavior and environmental vulnerability. The importance of analyzing large-scale patterns is related with the possibility of identifying extensive regions under similar possibility for fire spread, and most important, due to the AO/PNA predictability, the possibility of advanced identification of the environmental fire vulnerability may be determined.

Fires and AO/PNA in 2015–2020

According to the US National Interagency Fire Center the years 2015–2020 have experienced severe fires and unprecedent area burned (https://www.nifc.gov/fire-information/statistics/wildfires). Fire activity is enhanced globally as well[2,10] and in many countries such as Brazil, Russia, Australia and Canada ecosystem processes and vegetation have been seriously affected. Since 2015, the NASA fire product has improved the probability of detection of fires showing regionally an increase of ≈3% in North America and Asia compared to Collection 5. An 1% increase is noted across Equatorial Asia and Central Asia, and about 1% absolute decrease in South America above the Equator[43]. Thus, when comparing the fire activity between the 2001–2016 and 2015–2020 some differences may arise due to changes in the MODIS detection method. However, this should not affect analyses substantially because differences are not >3%.

In order to extend the PFIv2 analyses to 2017–2020 interval, the index is computed utilizing the CPC precipitation and temperature, and ERA5 relative humidity datasets. This allows for a better comparison between the two intervals. Anomalies are computed as differences through March–October between the 2001–2016 and 2015–2020 periods. The PFIv2 shows that most of central and western NA, Europe and northeastern Asia experience higher danger rating in the 2015–2020 interval, with respect to previous 2001–2016 averages (Fig. 7a). Large negative anomalies appear over southern Asia and Baltic countries (Fig. 7a).

Changes in precipitation over North America and Eurasia dictate the pattern of PFIv2 anomalies despite no significant trends of daily rainfall have been detected based on a Mann–Kendall test. However, changes are noticed on short-term accumulated precipitation as represented by DD. Indeed, over both regions, in particular northwestern North America and western Russia reduced DD (blue regions in Fig. 7b) in the 2015–2020 leads to the drop in PFIv2. However, across Siberia and Europe, temperature increases about 1–1.5 °C in the 2015–2020 interval with respect to 2001–2016, play an important role to result in positive anomalies.

These changes result in more fires across central Asia and western North America related to AO^+, and in western Russia/northeastern Europe, which have been more frequent during the PNA^+ phase (Fig. 7c, d). Despite being centered over western

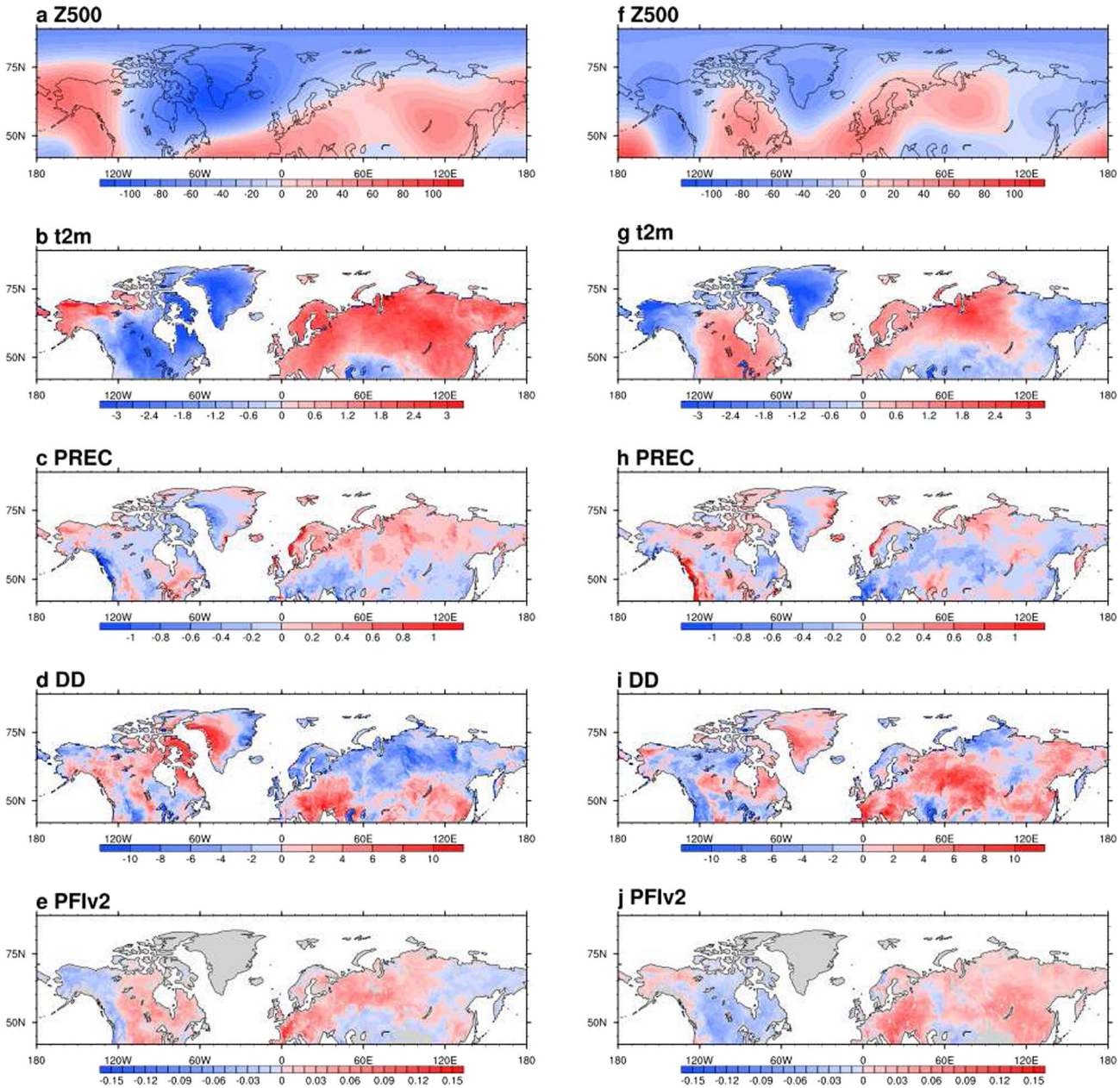

Fig. 6 Composite patterns due to AO+ and PNA+. a Z500 (mb), **b** surface temperature (C), **c** 15-day running mean precipitation (mm/day), **d** period of drought for the 2001–2016 interval. **e** is the PFIv2. **f**–**j** is the same as **a**–**e** but for coincident AO+ and PNA. Gray regions in **e** and **f** indicate sparse or absent vegetation.

North America and the eastern North Pacific Ocean, the PNA pattern has been responsible for inducing trends of burned areas in central Asia, as demonstrated by ref. [27]. It has to mentioned that the PNA is also well correlated with other climatic patterns such as East Pacific/North Pacific Oscillation, that can contribute to the fire occurrences as shown in Fig. 7d.

About 40% of detected fires in the 2015–2020 interval occurred under the positive phase of the AO, in particular over Asia. Positive AO and PNA with indices larger than 0.5 STD are found in 28% and 26% of 2015–2020 days, respectively. In Fig. 7e, f the total number of fires by gridbox and March–October differences between the two time intervals are shown. The analyses show that 2015–2020 has been marked by an increased number of hotspots in particular in western and central North America, southern and eastern Asia. The PFIv2 matches higher danger and fire occurrence[35] in some regions with sparse vegetation (savannas, open shrublands and grasslands), such as central and northern Asia. Across northern Europe and western Russia fire activity has been weakened as also demonstrated in the latter region by the PFIv2 anomalies (Fig. 7a, f). Mismatches between increased number of fires in the 2015–2020 and reduced fire danger rating during the same period indicate that increased precipitation is not sufficient to reduce the region vulnerability to ignition sources. Moreover, lower PFIv2 rating with respect to particular time do not direct imply in the absence of danger, because lower value may be still categorized within high fire danger level.

DISCUSSION

Despite the complexity of forecasting regional vulnerability to fire, wildfire managers can benefit from the predictability of AO and PNA. Positive or negative phases of these modes persist from a

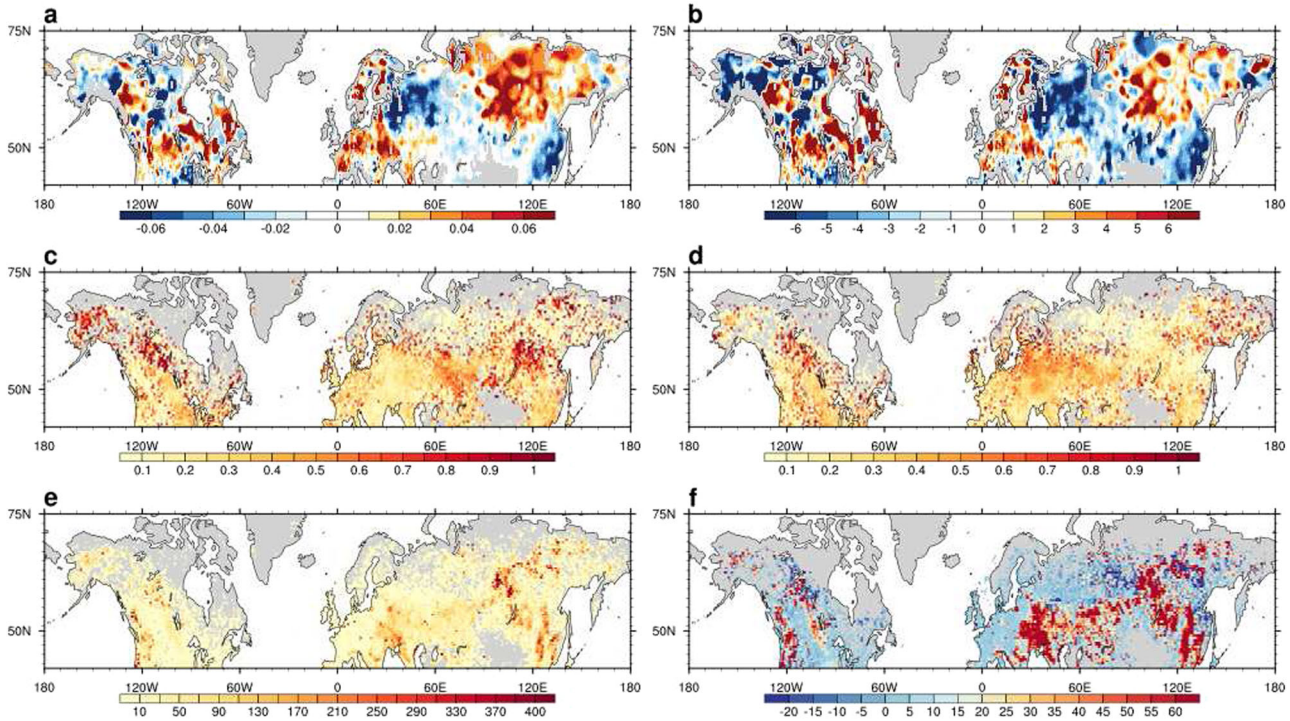

Fig. 7 Temporal changes of fires, PFIv2 and DD. Differences between PFIv2 averaged in 2015–2020 and 2001–2016 intervals (**a**). **b** shows the same as (**a**) but for differences in the period of drought (DD). **c** and **d** shows ratio between 2015 and 2020 accumulated fires during AO+ and PNA+ and the total number of fires in the period. **e** Total accumulated fires from 2015 to 2020. **f** shows differences between averaged annual fires between 2015–2020 and 2001–2016.

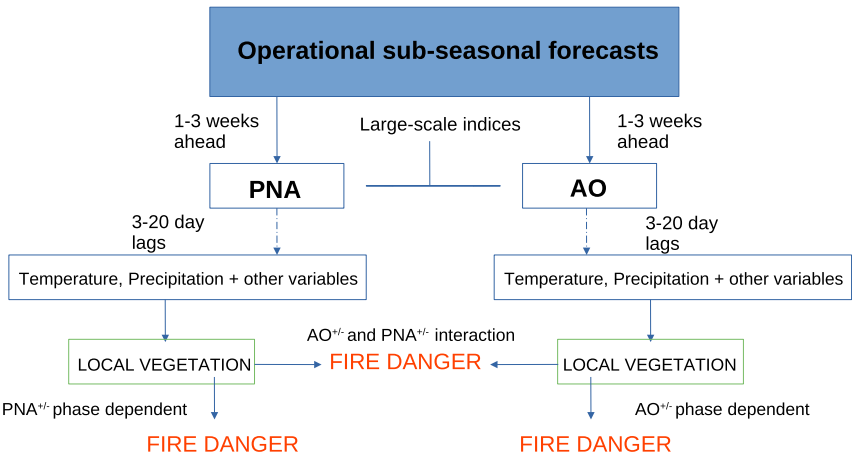

Fig. 8 Potential fire danger forecast. Flowchart summarizing the practical applications of the AO and PNA forecasts to fire danger management as a function of weather anomalies and local vegetation characteristics.

few days to a few months. Studies have shown that they can be predicted 2–3 weeks ahead, or for extended time scales, if external influences are assimilated into dynamical forecast models[44,45]. Results presented in our study demonstrate that AO/PNA leads hemispheric pattern of fire danger by 1–4 weeks. However, these modes induce surface local meteorological conditions depending on the dominant phase[37,46]. For instance, AO does not strongly impact the fire danger in Alaska, in opposition to PNA that dramatically increases danger (Fig. 1g, h). Thus, identification of the AO and PNA behavior in advance sheds light on future changes of the atmospheric susceptibility to fire occurrences, related to temperature and short-term precipitation anomalies. It should be added that local vegetation characteristics induce fuel loading which differ among sites, which per se, are related to modifications in fire danger ratings. This usefully serves to highlight the need for coupling large and local scales features insofar as fire vulnerability of a region is concerned (see Fig. 8).

The attribution of causes for changes in fire danger depends on the background vegetation, which in most situations is not well sampled. By assuming latitude–longitude grids, in particular over a hemispheric domain, high-resolution spatial data as used here can capture in more detail local surface characteristics. Although, consensus exists that weather characteristics are the main driving forcing for the environmental susceptibility to fire occurrences. Vegetation plays a determinant role for burned area extent and fire severity[10,47], and exerts important role because fuel loading and flammability are dependent on vegetation types. Limitation arises in the sense that parameterization of fuel amount related to

each plant type in response to drought, is extremely difficult because it also depends upon soil characteristics that are not available worldwide. The current study which is based on gridded state-of-the-art reanalyses, has no capability to provide results for individual vegetation cover. However, if weather station data and local vegetation are provided, the PFI is able to compute the fire danger rating.

Investigation conducted here explores the influence of weather anomalies induced by large-scale extratropical modes to accurately discretize the regional fire regimes. Moreover, it has also quantified the number of satellite-based fires which have been found under positive and negative fluctuations of the PNA and AO. The present study also contributes to previous analyses on the impact of other climate modes on fire activity[18–28]. The AO/PNA predictability is up to 3–4 weeks ahead and AO/PNA has been shown to lead the fire danger by up to 5–25 days (Fig. 8). This is a crucial finding as it does indicate that fire may occur if other variables are also in favor of fire ignition, and usefully serves to indicate preferential sites to be monitored. As demonstrated, by predicting these modes properly, higher fire danger rating and potential environmentally driven-fires can be anticipated in almost 90% of days in some locations. For instance, analyses to the 2015–2020 interval revealed that this period has experienced more fire incidence as compared to the 2001–2016, in particular in eastern and southern Asia, under the positive phase of the AO.

The current study does not cover all dimensions of fire variables, and for instance, the influence of lightning and humans which are known to play a significant role in frequency and severity of fires, are not addressed. These are complex issues and lightning certainly increases the environmental fire vulnerability whereas the human presence may lead to fire suppression. Future influence of humans has to be interpreted locally as it is a matter of collective conscience and engagement of relevant authorities in defining sustainable public policies. It is not speculative to argue that global warming can increase the impact of the AO and PNA as drivers of increased fire severity and frequency. In this sense, useful strategies to predict fire can be achieved by utilizing simulations that realistically can forecast the daily evolution of these modes. As demonstrated, they are in phase with increased number and very likely with the severity of fires across the Pan-Arctic, resulting in degraded environmental conditions, increased release of greenhouse gases to the atmosphere, and enhanced global warming.

METHODS

Climate data

This investigation applies satellite data and two state-of-the-art reanalyses. These reanalyses, which run under high resolution, are expected to capture essential environmental features related to fire incidence.

Initial analyses focus on weather elements and potential fire danger ratings variability to foresee the spatial and temporal evolution of those parameters. Subsequently, the use of soil moisture is linked to fire weather in order to review potential surface–atmosphere interaction that lead to increased environmental vulnerability. Two fire weather indices are used: FWI and the Potential Fire Index version 2 (PFIv2).

The second version of the Arctic System Reanalysis (ASRv2) is utilized as the climatic base for analyses in the present study from 2001 to 2016. The ASRv2 runs at 15 km horizontal resolution, and 71 model levels (29 pressure levels), with 27 surface and 10 upper air analysis variable being generated. Moreover, 74 surface and 16 upper air forecast variables, and 3 soil variables are also computed. The ASRv2 has been able to properly reproduce observed near-surface winds, temperature, precipitation, and tropospheric variables across the Pan-Arctic and extra-tropical region[48]. Radiative and turbulent fluxes have also been compared to site-specific measurements in which the high accuracy of ASRv2 has been demonstrated[49]. By applying the Arctic reanalysis to compute the potential fire danger rating based on the PFIv2 method, it has been demonstrated[35] that the ASRv2 delivers, with respect to ECMWF Reanalysis 5th Generation (ERA5), results in closer match with satellite based-hotspots. Daily extreme events that are crucial to characterize droughts, frost and heat wave susceptibility have also been evaluated across North America, in which is demonstrated that ASRv2 properly matches observations[9]. ASR data is available from NCAR RDA (https://rda.ucar.edu/datasets/ds631.1).

The CPC dataset (https://www.cpc.ncep.noaa.gov, last access: 28 October 2021), which includes weather stations and several additional observational data for precipitation and temperatures, has also been chosen for the PFIv2 calculation between 2001 and 2020, and the ERA5 relative humidity is currently used because this variable is not available in the CPC datasets.

The AO and PNA calculations are based on empirical orthogonal functions (EOF) analyses between 20°N and 90°N, applied upon NCEP/NCAR daily sea level pressure (SLP), and geopotential height at 500 hPa (Z500). Data used are at the $2° \times 2°$ latitude and longitude grid, from 2001 to 2020. The dominant hemispheric patterns of the AO and PNA are not expected to be drastically modified by using higher horizontal resolution to compute these modes. The first SLP principal component (PC) delivered by the EOFs is the AO, whereas the 2nd PC of Z500 is assumed as the PNA[40,50]. The AO (PNA) explains 16.8% (8.6%) of the variance of the data. A 15-day running mean is applied to reduced the high variability of the daily timeseries. It is worth mentioning that four harmonics of Fourier analysis are used to reconstruct a smoothed mean annual cycle. The use of harmonics may be understood as the ensemble of different sequences of annual cycles.

Thus, the single realization of our timeseries represents mean atmospheric conditions as expected based on much longer time interval. Since wildfire severity and occurrence in the NH are concentrated between March and October, calculations and discussions conducted herein are concentrated on these months. The ASRv2 has not been used to computed the AO and PNA due to its meridional extent, between 40°N and 90°N. However, the ASRv2 anomalies have been regressed upon the first and second components which characterize the AO and PNA. The high horizontal resolution across the Arctic and extra-tropical latitudes delivered by the ASRv2 should capture in more detail the link between fires and weather, as compared to lower resolution datasets that do not reproduce small scale processes in the spatial domain.

Satellite-based fires

The processed Moderate Resolution Imaging Spectroradiometer (MODIS) Collection 6 Near Real-Time (NRT) active fire products (Aqua + Terra) based on the standard MOD14DL/MYD14 fire and thermal anomalies algorithm have been used as fire proxies[43]. These data are available at https://earthdata.nasa.gov/earth-observation-data/near-real-time/firms (last access: August 2021). The MODIS hotspots (MCD14DL) are downloaded at 1 km resolution from 2001 to 2020. Analyses are conducted based on two intervals: 2001–2016 and 2015–2020. The 2015–2020 period has been characterized by more severe fires in particular across the Siberian region. These data are used to verify the relationship between fires, the modes of climate variability (PNA and AO) and soil moisture. It has to be mentioned that in exceptional cases hotspots can be identified in areas of high temperature such as oil chimneys, volcanoes, rocks or large sandbanks, however, it has been shown that these false identifications are rare[43] and represent a tiny fraction of the hotspot amounts. On the other hand, fires may be undetected due to thick smoke clouds as well as small size, and time occurrence. Nevertheless, the amount of missed fires may be very low as compared to the total, in particular in the current evaluation that deals with hemispheric domain, and 20 years of data. Validation has been conducted in South America on MODIS capacity to reproduce fires, and results demonstrated a good match between satellite-based hotspots and ground observations (https://queimadas.dgi.inpe.br/).

Potential fire danger rating, PFIv2

The PFIv2 has been described in other studies and for brevity only a summary is provided below[10,35]. The method relies on precipitation, temperature, atmospheric water vapor deficit and atmospheric stability at low levels, as a function of surface elevation according to a logistic function. This latter parameterization is important because fire vulnerability increases on the windward side of a slope and spreads into lower atmospheric pressure systems. The precipitation effect is computed as 11 intervals that characterizes its daily evolution within the preceding 120 days (namely: period of drought).

This is assumed because individual precipitation events, for instance 5 mm/day in the previous day, should not be taken as sufficient conditions

to extinguish the environmental susceptibility to fire development in the following days. To achieve an initial wildfire danger estimate, the period of drought (DD) is associated with the local vegetation because similar temporal distribution of precipitation delivers distinct environmental vulnerability to fire occurrence, which is dependent upon land cover characteristics. For instance, tundra and conifer respond differently to daily changes of precipitation, especially where litter or combustible material are concerned. The same applies to the drying out vegetation response to temperature. Plant opening and closing stomata and related evapotranspiration are dependent upon species characteristics and determine soil moisture water quantity[11]. The final PFIv2 equation

$$\mathrm{PFIv2} = \mathrm{BR}_{A_{1,16}} \times (a \times \mathrm{LogHai} + b) \times \mathrm{FT} \quad (1)$$

where $a = 0.006$ and $b = 1.3$, and $\mathrm{BR}_{A1,16} = 0.45 \times (1 + \sin(A_{1,16} \times \mathrm{DD}))$, where $A_{1,16}$ stands for 16 global vegetation types. The PFI method includes vegetation characteristics as provided by the vegetation data from annual MODIS MOD12C1 (https://lpdaac.usgs.gov/products/mcd12c1v006) and MCD12Q1 (https://lpdaac.usgs.gov/products/mcd12q1v006/) product observations, available from the Land Processes DAAC. The vegetation classes are parameterized as a flammability factor that evolves according to changes in short-term precipitation[10], leading to fire danger magnitude changes according to the land surface cover.

The FT takes into account temperature, namely $\mathrm{FT} = [0.02 \times Tx + 0.4) \times (0.003|\mathrm{Lat}| + 1)]$, where Tx is the maximum temperature and $|\mathrm{Lat}|$ stands for the grid latitude. In Eq. (1) the LogHai captures the influence of atmospheric stability[10], water pressure deficit and elevation on the PFIv2. The FT is included as a PFIv2 factor because similar air temperatures in the tropics and extra-tropics are associated with distinct vegetation responses in terms of production of litter and ignition material. In some areas this can lead to greening (Arctic) and others to browning, for instance in mid-latitudes. The PFIv2 varies from 0 to 1, such as: Minimum, below 0.15; Low, from 0.15 to 0.4; Medium, from 0.4 to 0.7; High, from 0.7 to 0.95 and Critical, above 0.95.

Fire weather index (FWI)

To provide additional information of fire danger rating the FWI is used. It has been retrieved from https://climate.copernicus.eu/fire-weather-index for the 2001–2020 period. The FWI is an index based on an empirical Canadian model widely used in many regions, and currently available at the European Forest Fire Information System (EFFIS). The FWI depends on wind speed, relative humidity and temperature and has been parameterized for regional applications. The FWI is categorized as such: very low (0.0 ± 5.2), low (5.2 ± 11.2), moderate (11.2 ± 21.3), high (21.3 ± 38.0), very high (38.0 ± 50.0), and extreme (50.0 ± 100.0). A critical issue related to the FWI is the lack of proper treatment of the individual vegetation flammability, such as of forest, savannas and grassland. For instance, the FWI may deliver the same danger for different vegetation types that are under similar weather conditions. This drawback results in misrepresentation of incidence of fires and higher values of FWI in arid and some locations northward of 40°N[35,51]. Additional details on FWI is found at https://cwfis.cfs.nrcan.gc.ca/background/summary/fwi.

DATA AVAILABILITY

The FWI is available at https://cwfis.cfs.nrcan.gc.ca/background/summary/fwi and the satellite-based fires at https://earthdata.nasa.gov/earth-observation-data/near-real-time/firms. All additional data to perform the analyses are available upon reasonable request from the corresponding author (fjustino@ufv.br).

CODE AVAILABILITY

All additional codes needed to perform the analyses are available upon reasonable request from the corresponding author (fjustino@ufv.br).

Received: 19 January 2022; Accepted: 27 May 2022;
Published online: 24 June 2022

REFERENCES

1. Natali, S. M. et al. Permafrost carbon feedbacks threaten global climate goals. *Proc. Natl. Acad. Sci. USA* **118**, https://doi.org/10.1073/pnas.2100163118 (2021). https://www.pnas.org/content/118/21/e2100163118.full.pdf.
2. Zhang, Z., Wang, L., Xue, N. & Du, Z. Spatiotemporal analysis of active fires in the Arctic Region during 2001–2019 and a Fire Risk Assessment Model. *Fire* **4**, https://doi.org/10.3390/fire4030057 (2021).
3. Lasslop, G. & Kloster, S. Human impact on wildfires varies between regions and with vegetation productivity. *Environ. Res. Lett.* **12**, 115011 (2017).
4. Yue, C. et al. Modelling the role of fires in the terrestrial carbon balance by incorporating spitfire into the global vegetation model orchidee. Part 1: simulating historical global burned area and fire regimes. *Geosci. Model. Dev.* **7**, 2747–2767 (2014).
5. Knorr, W., Kaminski, T., Arneth, A. & Weber, U. Impact of human population density on fire frequency at the global scale. *Biogeosciences* **11**, 1085–1102 (2014).
6. Jain, P., Castellanos-Acuña, D., Coogan, S., Abatzoglou, J. & Flannigan, M. Observed increases in extreme fire weather driven by atmospheric humidity and temperature. *Nat. Clim. Chang*. https://doi.org/10.1038/s41558-021-01224-1 (2021).
7. Walker, X. J. et al. Increasing wildfires threaten historic carbon sink of boreal forest soils. *Nature* **572**, 520–523 (2019).
8. Veraverbeke, S. et al. Lightning as a major driver of recent large fire years in North American boreal forests. *Nat. Clim. Chang*. **7**, https://doi.org/10.1038/nclimate3329 (2017).
9. Avila-Diaz, A., Bromwich, D. H., Wilson, A. B., Justino, F. & Wang, S.-H. Climate extremes across the North American Arctic in modern reanalyses. *J. Clim.* **34**, 2385–2410 (2021).
10. da Silva, A. S., Justino, F., Setzer, A. W. & Avila-Diaz, A. Vegetation fire activity and the Potential Fire Index (PFIv2) performance in the last two decades (2001 ± 2016). *Int. J. Climatol.* **41**, E78–E92 (2021). https://rmets.onlinelibrary.wiley.com/doi/pdf/10.1002/joc.6648.
11. Lian, X. et al. Summer soil drying exacerbated by earlier spring greening of northern vegetation. *Sci. Adv.* **6**, eaax0255 (2020).
12. Vivoni, E. R. et al. Observed relation between evapotranspiration and soil moisture in the North American monsoon region. *Geophys. Res. Lett.* **35**, https://doi.org/10.1029/2008GL036001 (2008) https://agupubs.onlinelibrary.wiley.com/.
13. Wang, J., Liu, D., Ciais, P. & Penuelas, J. Decreasing rainfall frequency contributes to earlier leaf on set in northern ecosystems. *Nat. Clim. Chang*. https://doi.org/10.1038/s41558-022-01285-w (2022).
14. Harrington, T. S., Zhu, J. & Skinner, C. B. Terrestrial sources of summer arctic moisture and the implication for arctic temperature patterns. *npj Clim. Atmos. Sci.* **4**, 1–14 (2021).
15. Ault, T., Macalady, A., Pederson, G., Betancourt, J. & Schwartz, M. Northern hemisphere modes of variability and the timing of spring in western North America. *J. Clim.* **24**, 4003–4014 (2011).
16. York, A. et al. *Wildland Fire in High Northern Latitudes*. Administrative Report, Corporate Authors(s) (Alaska Center for Climate Assessment and Policy (U.S.); International Arctic Research Center; University of Alaska Fairbanks, United States. National Oceanic and Atmospheric Administration. Office of Oceanic and Atmospheric Research; Cooperative Institute for Research in the Atmosphere, Fort Collins, CO, 2020).
17. Ju, J. & Masek, J. G. The vegetation greenness trend in Canada and US Alaska from 1984–2012 Landsat data. *Remote Sens. Environ.* **176**, 1–16 https://doi.org/10.1016/j.rse.2016.01.001.
18. Abatzoglou, J. T. & Williams, A. P. Impact of anthropogenic climate change on wildfire across western US forests. *Proc. Natl. Acad. Sci. USA* **113**, 11770–11775 (2016)
19. Zhuang, Y., Fu, R., Santer, B. D., Dickinson, R. E. & Hall, A. Quantifying contributions of natural variability and anthropogenic forcings on increased fire weather risk over the western United States. *Proc. Natl. Acad. Sci. USA* **118**, https://doi.org/10.1073/pnas.2111875118 (2021). https://www.pnas.org/content/118/45/e2111875118.full.pdf.
20. Jolly, W. M. et al. Climate-induced variations in global wildfire danger from 1979 to 2013. *Nat. Commun.* **6**, 1–11 (2015).
21. Le Page, Y. et al. Global fire activity patterns (1996–2006) and climatic influence: an analysis using the World Fire Atlas. *Atmos. Chem. Phys.* **8**, 1911–1924 (2008).
22. Mason, S. A., Hamlington, P. E., Hamlington, B. D., Matt Jolly, W. & Hoffman, C. M. Effects of climate oscillations on wildland fire potential in the continental United States. *Geophys. Res. Lett.* **44**, 7002–7010 (2017).
23. Greenville, A. C., Dickman, C. R., Wardle, G. M. & Letnic, M. The fire history of an arid grassland: the influence of antecedent rainfall and ENSO. *Int. J. Wildland Fire* **18**, 631–639 (2009).
24. Dixon, P. G., Goodrich, G. B. & Cooke, W. H. Using teleconnections to predict wildfires in Mississippi. *Mon. Weather. Rev.* **136**, 2804–2811 (2008).
25. Churakova Sidorova, O., Siegwolf, R., Fonti, M., Vaganov, E. & Saurer, M. Spring arctic oscillation as a trigger of summer drought in Siberian subarctic over the past 1494 years. *Sci. Rep.* **11**, https://doi.org/10.1038/s41598-021-97911-2 (2021).

26. Kim, J.-S., Kug, J.-S., Jeong, S.-J., Park, H. & Schaepman-Strub, G. Extensive fires in southeastern siberian permafrost linked to preceding arctic oscillation. *Sci. Adv.* **6**, eaax3308 (2020).
27. Shi, K. & Touge, Y. Characterization of global wildfire burned area spatiotemporal patterns and underlying climatic causes. *Sci. Rep.* **12**, https://doi.org/10.1038/s41598-021-04726-2.
28. Zheng, C., Bolan, G., Lixin, W. & Fan, J. Pacific-North American teleconnection and North Pacific Oscillation: historical simulation and future projection in CMIP5 models. *Clim. Dyn.* **50**, 4379–4403 (2017).
29. Yu, B. & Zwiers, F. The impact of combined ENSO and PDO on the PNA climate: a 1,000-year climate modeling study. *Clim. Dyn.* **29**, 837–851 (2007).
30. Thompson, D. W. J. & Wallace, J. M. Regional climate impacts of the Northern Hemisphere annular mode. *Science* **293**, 85–89 (2001).
31. Justino, F., Gurjão, C. & Lindemann, D. Climate response to drastically modified PDO, PNA and NAM in the superinter- glacial MIS 31. *Boreas* https://doi.org/10.1111/bor.12556 (2021). https://onlinelibrary.wiley.com/doi/pdf/10.1111/bor.12556.
32. Hamouda, M. E., Pasquero, C. & Tziperman, E. Decoupling of the Arctic Oscillation and North Atlantic Oscillation in a warmer climate. *Nat. Clim. Chang.* **11**, 137–142 (2021).
33. Chen, Y. et al. Future increases in Arctic lightning and fire risk for permafrost carbon. *Nat. Clim. Chang.* **11**, 404–410 (2021).
34. Sato, T. & Nakamura, T. Intensification of hot eurasian summers by climate change and land±atmosphere interactions. *Sci. Rep.* **9**, 10866 (2019).
35. Justino, F. et al. Estimates of temporal–spatial variability of wildfire danger across the Pan-Arctic and extra-tropics. *Environ. Res. Lett.* **16**, 044060 (2021).
36. Park, H.-J. & Ahn, J. B. Combined effect of the Arctic Oscillation and the Western Pacific pattern on East Asia winter temperature. *Clim. Dyn.* **46**, https://doi.org/10.1007/s00382-015-2763-2 (2015).
37. Harding, K. J. & Snyder, P. K. The Relationship between the Pacific±North American Teleconnection Pattern, the Great Plains Low-Level Jet, and North Central U.S. Heavy Rainfall Events. *J. Clim.* **28**, 6729–6742 (2015).
38. Wallace, J. M. & Gutzler, D. S. Teleconnections in the geopotential height field during the Northern Hemisphere winter. *Mon. Weather Rev.* **109**, 784–812 (1981).
39. Loikith, P. C. & Broccoli, A. J. The influence of recurrent modes of climate variability on the occurrence of winter and summer extreme temperatures over North America. *J. Clim.* **27**, 1600–1618 (2014).
40. Thompson, D. W. J. & Wallace, J. M. Annular Modes in the Extratropical Circulation. Part I: Month-to-Month Variability. *J. Clim.* **13**, 1000–1016 (2000).
41. Sidorova, O. V., Siegwolf, R. T., Fonti, M. V., Vaganov, E. A. & Saurer, M. Spring arctic oscillation as a trigger of summer drought in Siberian subarctic over the past 1494 years. *Sci. Rep.* **11**, 1–10 (2021).
42. Cai, L., Alexeev, V. A., Walsh, J. E. & Bhatt, U. S. Patterns, impacts, and future projections of summer variability in the Arctic from CMIP5 models. *J. Clim.* **31**, 9815–9833 (2018).
43. Giglio, L., Schroeder, W. & Justice, C. O. The collection 6 MODIS active fire detection algorithm and fire products. *Remote Sens. Environ.* **178**, 31–41 (2016).
44. Domeisen, D. I. V., Badin, G. & Koszalka, I. M. How predictable are the Arctic and North Atlantic Oscillations? Exploring the variability and predictability of the Northern Hemisphere. *J. Clim.* **31**, 997–1014 (2018).
45. Kim, H.-J. & Ahn, J.-B. Improvement in prediction of the Arctic Oscillation with a realistic ocean initial condition in a CGCM. *J. Clim.* **28**, 8951–8967 (2015).
46. Zhang, J. et al. Analysis of the positive Arctic Oscillation Index Event and Its influence in the winter and spring of 2019/2020. *Front. Earth Sci.* **8**, https://doi.org/10.3389/feart.2020.580601 (2021).
47. Bowman, D. M. J. S. et al. Vegetation fires in the Anthropocene. *Nat. Rev. Earth Environ.* **1**, 500–515 (2020).
48. Bromwich, D. et al. The Arctic system reanalysis, version 2. *Bull. Am. Meteorol. Soc.* **99**, 805–828 (2018).
49. Justino, F. et al. Northern Hemisphere extratropical turbulent heat fluxes in ASRv2 and global reanalyses. *J. Clim.* **32**, 2145–2166 (2019).
50. L'Heureux ML., Kumar, A., Bell, G. D., Halpert, M. S. & Higgins, R. W. Role of the Pacific-North American (PNA) pattern in the 2007 Arctic sea ice decline. *Geophys. Res. Lett.* **35**, https://doi.org/10.1029/2008GL035205 (2008). https://agupubs.onlinelibrary.wiley.com/.
51. Bedia, J. et al. Global patterns in the sensitivity of burned area to fire-weather: implications for climate change. *Agric. Meteorol.* **214**, 369–379 (2015).

ACKNOWLEDGEMENTS

F.J. thanks the Fulbright Foundation, the Byrd Polar Climate and Research Center (BPCRC), as well as the Brazilian National Council for Scientific and Technological Development (CNPq, grant number 442577/2020-6), for financial support. Contribution number C-1617 of Byrd Polar and Climate Research Center.

AUTHOR CONTRIBUTIONS

F.J. and D.B. wrote most of manuscript and analyzed results, A.S. and V.S. computed the PFIv2, retrieved and processed observed fire, S.H. analyzed the results and contributed with discussion. All authors reviewed the manuscript.

COMPETING INTERESTS

The authors declare no competing interests.

ADDITIONAL INFORMATION

Supplementary information The online version contains supplementary material available at https://doi.org/10.1038/s41612-022-00274-2.

Correspondence and requests for materials should be addressed to Flavio Justino.

Reprints and permission information is available at http://www.nature.com/reprints

Publisher's note Springer Nature remains neutral with regard to jurisdictional claims in published maps and institutional affiliations.